NORSAR

NORSAR Scientific Report No. 1-2002

Semiannual Technical Summary

1 July - 31 December 2001

Frode Ringdal (ed.)

Kjeller, February 2002

6.5 Comparison of location procedures – The Kara Sea event of 16 August 1997

Introduction

A seismic event in the Kara sea to the east of Novaya Zemlya on 16 August 1997 has been the subject of considerable discussion, because the very limited set of stations available to the International Seismological Centre (ISC) and the Reviewed Event Bulletin (REB) of the Experimental International Data Centre (EIDC) are inadequate to constrain the depth effectively. Could this event have been an underwater explosion?

A more comprehensive data set has been assembled by repicking all available records from the event, including the station AMD at the northern end of the Urals which lies the closest to the event at about 400 km range. The distribution of seismic stations, which observed this event is shown in Fig. 6.5.1, the station coordinates are listed in Table 6.5.1, and the full phase list with arrival time, slowness and azimuth readings are presented in Table 6.5.2.

Many of the stations lie in Fennoscandia, but azimuthal control is improved by a set of stations in the western Barents Sea and in Russia. The total data set contains many S readings; even where these have significant reading uncertainties (see Table 6.5.2), they can help to provide control on position and depth through the sensitivity of the differential S-P times to distance.

A sequence of location experiments have been undertaken to compare the results of using both different velocity models to describe the travel times of the phases and also to make a comparison between the use of a linearized location algorithm (HYPOSAT – Schweitzer, 2001) and a fully non-linear scheme (shakeNA – Sambridge and Kennett, 2001). For direct comparisons between the two methods we have used a standard least-squares misfit criterion, but have also examined the influence of more robust choices for data misfit when using the non-linear location scheme.

Observed data and tested models

We have employed the global reference models *JB* (Jeffreys and Bullen, 1940), *PREM* (Dziewonski and Anderson, 1981), *IASP91* (Kennett and Engdahl, 1991), and *AK135* (Kennett *et al.*, 1995), and also considered two regional models derived from the *Barents* model of Kremenetskaya *et al.* (2001). The *barey* model is very similar to the *Barents* model with a P- to S-velocity ratio close to 1.78, while the *barez* model has identical P velocities as *barey* model but faster S wavespeed with a P- to S-velocity ratio of 1.72 (see Fig. 6.5.2). We have found that the *barey* model gives a good representation of paths from the Kara Sea to Fennoscandia but that the *barez* model is more suitable for paths from the Kara Sea to Spitsbergen, Bear Island, and to Northern Siberia.

All of the listed observations in Table 6.5.2 were used during our study. However, the final inversions were made without some of these data: The S onsets at KTK1 and TRO were not used because we had no direct P observation of these in trigger mode operated stations. The P onset at MOR8 was not used because we suspect an absolute timing error at MOR8 (for all inversion results the residuum of this P onset is anomalously large). The ISC used a reading for NB2, which is a reported analysis on the beam calculated for the whole NORSAR array. Instead of recalculating this beam, we analyzed the onsets individually on all available 3C

broadband traces (NAO01, NB201, NC303, and NC602) of the NORSAR array. However, NC602 is co-located with the centre element (NRA0) of the NORES array and therefore we skipped the NC602 reading for our final analyses. The pIDC published in the REB an Sn-onset time for station ARU. We requested the ARU data from the pIDC to reanalyze also these records. However, after carefully checking the 3C data around the presumed and reported onset time, we could not confirm any Sn onset from the theoretically backazimuth and rejected this reading. However, this spurious onset was also listed in the ISC bulletin but never used as defining observation at the EIDC or at the ISC. Our final inversion therefore employs 23 P-phase and 13 S-phase readings from 23 different seismic stations at a distance range of about about 3˚ to 21˚.

Results with the Neighbourhood Algorithm shakeNA

The non-linear location procedure using the Neighbourhood Algorithm (NA) is based on an exploration of the 4-D hypocentral parameter space to find models with good fit to the data. At each stage the algorithm makes use of all the prior information to define a partition of the parameter space into Voronoi cells around each sampled point describing the region which lies closest to that point. To find effective location estimates the algorithm is used in a fairly focused way with an initial sampling of 9 points in the entire specified volume and then 9 new points in each iteration randomly sampling the current two “best” Voronoi cells, *i.e.* those containing the points with the least misfit. In this mode the progress of the non-linear inversion resembles the convergence of a cloud of points towards single goal.

The NA scheme was applied to a zone 16 deg across in longitude and 8 deg across in latitude and extending to 120 km deep, centred in the Kara Sea, and up to 20 s variation in origin time was also allowed. Despite the large initial domain convergence is rapid and low misfits can readily be achieved in about 30 iterations. The misfit levels for the two global reference models *AK135*, *IASP91* is comparable but *AK135* provides a slightly better fit. A variance reduction of about 30% can be achieved by using the region-specific models, *barey* and *barez.*

In Fig. 6.5.3 we show the central portion of the parameter space (a 20 km square about the same reference point) for the *barez* model. The NA algorithm has been extended here to 60 iterations to provide a further exploration of the zone of better misfit, the group of black models have a very similar level of misfit and define a ‘consistency region’ indicated with the gray polygons which indicates the variability allowed in the event location. This consistency region is defined with the aid of an auxiliary weighting function, based on analogues from statistical physics. It is easier to derive a threshold scheme for the weighting function than for the misfit itself, because the shape of the weighting function is known and only scaling varies. There is only a marginal difference between the levels of misfit for the solutions indicated with black symbols. The solution with best fit to data is indicated with the open diamond, but a more useful quantity is generally the ensemble weighted average indicated with the gray cross.

We believe that the robust statistic tends to suppress the influence of outliers and in doing so finds an alternative region of good fit with a different combination of depth and origin time. The sensitivity of the data misfit to subareas of the hypocenter space and indeed groups of solutions with very similar levels of misfit can exist. This is illustrated with Fig. 6.5.4, where we show the central portion of the parameter space for model *IASP91*. Clearly subregions of equally good misfit levels can be identified, notably in depth.

The epicentral areas of all four models tested with the NA algorithm are plotted in Fig. 6.5.5 and Table 6.5.3 lists the corresponding numerical results. The polygons give always the consistency region of the solution for each model. In addition two plotted two solutions: once the one with the absolute minimal misfit as open symbols and once the mean of the whole assemble of solutions defining the 'consistency region' as small filled symbols. The shakeNA locations for the standard Earth models *IASP91* and *AK135* are very close and clearly separated by about 20 km from the solutions using the regional models *barey* and *barez*, the latter show somewhat smaller consistency regions.

For a quantitative measure of the quality of an event location we have calculated two different parameters: the root-mean square (RMS) of all defining onset times and a weighted mean misfit of all observed parameters (WMF). The WMF values are calculated by calculating the mean of the residuals weighted by the standard deviation of the observation. RMS and WMF are also listed for each hypocenter determination in Table 6.5.3.

The presence of sets of solutions with very similar levels of fit poses problems when using a linearized inverse scheme because the algorithm will tend to be pulled towards one particular epicentral subregion or depth range (*e.g.* depending on where it was initiated), and unlike the non-linear scheme will not be able to escape to find a better point. If we are unlucky there is the possibility of approaching the minimum from a direction such that the next iteration overshoots its target and then returns to near the earlier point at the subsequent iteration. Such oscillations are difficult to tame.

In both, the non-linear and the linearized inversions, we found that the patterns of residuals when using either the *barey* or *barez* models reveal an inconsistency for S waves between paths to Spitsbergen and Siberia one side and Fennoscandia on the other side. Either one group or the other group of paths is well fitted, but always with significant residuals for the second group. This suggests the use of different models for the two sets of paths.

Discussion of the HYPOSAT results

To get the results of the HYPOSAT inversions comparable with the shakeNA results, the HYPOSAT inversions were restricted to a strict least-squares scheme without using special stations corrections or travel-time differences between the phases observed at one stations. All error ellipses for the epicenter were calculated for a 90% significance level after projecting the corresponding uncertainties of source time and event depth in consideration of the covariance matrix into the epicentral-error space. The iteration process was stopped when two sequential solutions were closer than 0.5 km to each other. To force a stable result, the program itself removes some observations during the iterations of the inversion when the residuals became too large. Therefore the number of defining parameters changes slightly for the different solutions.

We tested the same models as for the shakeNA scheme. The epicenters are plotted together with the shakeNA results in Fig. 6.5.5, and Table 6.5.3 again lists the corresponding numbers. The HYPOSAT epicenters are plotted with large filled symbols and their corresponding error ellipses as broken lines. The error ellipses and epicenters for the standard Earth models *IASP91* and *AK135* overlap very well with the shakeNA results. However, because of the inadequate velocity models, for both models the inversions were oscillating between a source depth in the middle crust and below the Mohorovicic discontinuity and the program fixed the depth.

Because of this source parameter reduction we also get a dimension reduction of the covariance matrix and consequently relatively small error ellipses, although the RMS and WMF values are relatively large.

For the models *barey* and *barez* the data were consistent enough that HYPOSAT inverted also for the event's depth. As in case of shakeNA, the models can only explain a subset of data, depending on the actual ray paths. For *barey* the S-phase observations on Spitsbergen and on the Bear Island could not be modeled and the error ellipse become very large. The hypocenter itself lies within the shakeNA results. For *barez* all residuals of the S observations in Fennoscandia became very large and were refused as defining parameters. Consequently, the data set became more homogeneous and the error ellipse smaller. The agreement with the shakeNA solutions for *barez* is worse but both the consistency region and the error ellipse show some overlap.

The data set for this Kara Sea event shows a bimodal distribution in observed travel times. Therefore, the original HYPOSAT code was extended such that it can now jointly apply two different travel-time tables after choosing the best travel-time table for each path (see Table 6.5.2). For a final solution — here called *comb* (Fig. 6.5.5, in red) — we applied all possibilities of HYPOSAT (i.e. station elevation corrections, inverting for travel-time differences, and choosing the travel-time table with respect to the paths) and the result was a location with a very small error ellipse and very small data residuals.

To find out, how sensitive our *comb* location is for data from the nearest station AMD, we ran several tests. Starting with a depth of 0 km, we inverted the data with different combinations of AMD contributions, *i.e.* without any AMD observations, only with the Pn or only with the Sn onset, and with both onsets with or without also inverting the travel-time difference Sn-Pn. The result of these tests was that only if we include **both** the Pn and the Sn onset time (in any combination) at AMD, we could resolve the event depth as about 20 km.

Finally, we tested if the source depth as estimated for solution *comb* is depending on the start depth of the inversion. Therefore a start solution close to the epicentral area with start depth of 0, 10, 20, and 30 km was chosen for the inversion. In all cases the inversion converged to a depth between 15 and 20 km and using the start depth as fixed depth the result for 20 km had the smallest residuals.

In conclusion, the location estimations from the different techniques agree quite well and show some overlap of their confidence regions or error ellipses. From this we conclude that the event cannot be shallower than 10 km and is most likely in the lower crust at about 20 km depth.

Comparison with data centre solutions

The international data centres pIDC (REB), NEIC (PDE), and ISC located the discussed Kara Sea event. They all used slightly different observations and published different solutions. All these solutions are listed in Table 6.5.4, and Fig. 6.5.6 shows the epicenters (REB: diamond, PDE: hexagon, ISC: point) with their published error ellipses in black together with our *comb* solution for all available data in red (see Table 6.5.3). The number of defining observations for the ISC location is relatively large because the ISC used in its inversion the data from the arrays SPITS, FINES, and NORES twice as defining: once under the array-beam name and once under the name of the central site of the array (SPA0, FIA0, and NRA0).

The precise travel-time curves, location algorithms and applied data uncertainties of the data centre solutions are unknown to us. Therefore, it is difficult to compare our solutions with the data centre solutions. We choose the following approach for our experiment: to use only those of our readings, which were made at the same stations as listed in the ISC bulletin (all entries marked with a 'C' in Table 6.5.2). Then we relocated the event (see Fig. 6.5.6 and Table 6.5.1) with HYPOSAT for the different standard Earth models *JB* (Jeffreys and Bullen, 1940, gray, point), *PREM* (Dziewonski and Anderson, 1981, blue, hexagon), *IASP91* (Kennett and Engdahl, 1991, red, triangle), and *AK135* (Kennett *et al.*, 1995, blue, square) and for the three models derived for the Barents Sea region (*barey* (rhomb), *barez* (triangle), and *comb* (point), all in green), where *comb* is again the combined usage of *barey* and *barez*.

Because this subset of data have no resolution for the event's depth, we used here a fixed depth of 18 km which came from our *comb* solution for the whole data set. In addition we listed in Table 6.5.4 the number of defining parameters used for the locations, the RMS values of all as defining used onset times, and the epicentral distance to our *comb* solution from table Table 6.5.3. To get some feeling about the quality of the different solution we calculated again the WMF values. For the data centre solutions we used the data uncertainties as given in Table 6.5.2 but the residuals as published in the bulletins. In the REB as well as in the ISC bulletin an Sn reading from station ARU is listed but was not used to locate the event. To calculate the WMF value for the REB solution, this residual of -20.8 s was ignored.

All relocations for the three global models *JB*, *IASP91*, and *AK135* are very close and from the data centre solutions only the REB solution lies within their definitely larger error ellipses. The relatively small error ellipse of the REB solution is mainly because the Sn onsets with their large residuals were not used as defining for the solution. In our relocations (including *PREM*) all onsets were used and contribute with their residuals to the larger error ellipses. In all these solutions the P-type onsets are more or less equally well explained but not the Sn onsets. Because this could be a depth effect we also relocated the event with a fixed depth at 0 km and at 10 km. For all four global models (*JB*, *PREM*, *IASP91*, and *AK135*) the residuals were smallest for the fixed depth at 18 km.

The smallest residuals were obtained for the new regional models (see the green locations on the map). The worst of these solutions is for model *barez*, of which we know that it explains best the readings from stations in the western Barents Sea, at AMD, and at NRIS. The subset of data, used in this experiment, contains such readings only from the SPITS array. All other readings are from Fennoscandia or the Kola Peninsula. For these data model *barey* explains better the Sn-onset times. Consequently the location with model *barey* has smaller residuals. The residuals and the error ellipse for model *comb* are the smallest and this solution is the closest to our *comb* solution. This is a clear effect of using path specific velocity models.

Conclusion

This study has shown both the importance of S wave information in assessing the depth of regional events, and the need to get a good regional velocity model for both P and S in order to place the strongest constraints on the location of the event.

The conclusions from our experiment of comparing the different data centre solutions with our results are that using only a limited data set but an adequate travel-time model one can locate the event in the Kara Sea relatively close to our *comb* location. In this case the depth resolution

is of course negligible. The relative small error ellipses are a problem which arises when using only a limited number of data. Then the data errors do not usually follow a normal distribution but are biased in one direction and suggest high resolution and accuracy.

The location estimates for the whole data set from the different techniques agree quite well, with some overlap of the estimated confidence regions. The event cannot be shallower than 10 km and is most likely in lower crust around 20-30 km depth. Such deep crustal events are often attributed to the long-term effects of ice-unloading from the last glaciation and were previously observed around Novaya Zemlya (*e.g.* Marshall *et al.,* 1989). That this event was not an underwater explosion is also confirmed by the occurrence of an aftershock in the same epicentral area about four hours later (Ringdal *et al.,* 1997) and the fact that the observed seismic signals do not show bubble pulse reverberations, typical for underwater explosions.

Johannes Schweitzer

Brian Kennett, RSES, Australian National University

References

Dziewonski, A.M. and Anderson D.L. (1981): Preliminary reference Earth model. Phys. Earth Planet. Inter. **25**, 297-356.

Jeffreys, H., and Bullen, K.E., (1940): Seismological tables. British Association for the Advancement of Science, London 1940, 50 pp.

Engdahl, E.R., R. van der Hilst, and R. Buland (1998): Global teleseismic earthquake relocation with improved travel times and procedures for depth determination. Bull. Seism. Soc. Amer. **73**, 1271-1302.

Kennett, B.L.N., and Engdahl, E.R. (1991): Travel times for global earthquake location and phase identification. Geophys. J. Int. **105**, 429-466.

Kennett, B.L.N., Engdahl, E.R., and Buland, R. (1995): Constraints on seismic velocities in the Earth from traveltimes. Geophys. J. Int. **122**, 108-124.

Kremenetskaya, E., V. Asming, and F. Ringdal (2001): Seismic Location Calibration of the European Arctic. Pure appl. geophys. **158**, 117-128.

Marshall, P.D., R.C. Stewart, and R.C. Lilwall (1989): The seismic disturbance on 1986 August 1 near Novaya Zemlya: A source of concern? Geophys. Jour. Int. **98**, 565-573.

Ringdal, F., T. Kværna, E.O. Kremenetskaya, and V.E. Asming (1997): The seismic event near Novaya Zemlya on 16 August 1997. In: NORSAR Semiannual Tech. Summ. 1 April - 30 September 1996, NORSAR Sci. Rep. **1-97/98**, Kjeller, Norway, 110-119.

Sambridge, M.S., and B.L.N. Kennett (2001): Seismic Event Location: Nonlinear Inversion Using a Neighbourhood Algorithm. Pure appl. geophys. 1**58**, 241-257.

Schweitzer, J. (2001): HYPOSAT – An enhanced routine to locate seismic events. Pure appl. geophys. **158**, 277-289.

Table 6.5.1. Stations and their coordinates used in this study (see also Fig. 6.5.1). A star indicates if the reading(s) of this station were used or listed by international agencies or in this study.

Station	Latitude [˚]	Longitude [˚]	Elevation [m]	PIDC	NEIC	ISC	This study
AMD	69.7667	61.6833	200.0	-	-	-	*
APA0	67.6061	32.9931	200.0	-	-	*	*
ARU	56.4302	58.5625	250.0	*	-	*	-
BJO	74.5055	19.1883	18.0	-	-	-	*
FINES	61.4436	26.0771	150.0	*	*	*	*
HFS	60.1342	13.6956	265.0	*	*	*	*
JOF	62.9182	31.3124	180.0	-	-	-	*
KAF	62.1128	26.3061	205.0	-	*	*	*
KBS	78.9256	11.9417	74.0	-	-	-	*
KEF	62.1672	24.8703	215.0	-	-	-	*
KEV	69.7553	27.0067	81.0	-	-	-	*
KJN	64.0853	27.7119	250.0	-	-	-	*
KTK1	69.0117	23.2371	340.0	-	-	*	*
MOR8	66.1713	14.4411	445.0	-	-	*	*
NAO01	60.8442	10.8865	426.0	-	-	-	*
NB201	61.0495	11.2939	613.0	-	-	-	*
NB2	61.0397	11.2148	717.0	-	-	*	-
NC303	61.2251	11.3690	401.0	-	-	-	*
NC602	60.7353	11.5414	305.0	-	-	-	*
NORES	60.7353	11.5414	302.0	*	*	*	*
NRIS	69.0061	87.9964	498.0	*	*	*	*
NUR	60.5090	24.6514	102.0	-	*	*	*
PKK	60.0052	24.5169	10.0	-	-	-	*
PVF	60.5451	25.8616	45.0	-	-	-	*
SDF	67.4203	26.3936	276.5	-	-	-	*
SPITS	78.1777	16.3699	323.0	*	*	*	*
SUF	62.7192	26.1506	185.0	-	-	-	*
TRO	69.6325	18.9281	15.0	-	-	*	*
VAF	63.0422	22.6715	55.0	-	-	-	*

Table 6.5.2. All reread parameters as onset times, backazimuths (BAZ), and ray parameters (P) and their standard deviations σ of first P- and S-type onsets. Epicentral distances (Δ) and azimuths (AZI) were calculated with respect to the *comb* solution of Table 6.5.3. To find this and all other solutions of this table, all with an 'I' marked data were inverted. For the *comb* solutions, we used model *barey* for all travel-time relevant parameters except for the observations indicated with a '2' - in this case model *barez* was applied. A 'C' marks data used for the comparison of the results of this study with the solutions published by international data centres (see Table 6.5.4).

Station	Δ [°]	AZI [°]	Phase	Hour	Minute	Second	σ Time [s]	BAZ [°]	σ BAZ [°]	P [s/°]	σ P [s/°]	Remarks
AMD	2.917	151.2	P	02	11	48.50	0.10	-	-	-	-	I-2
AMD	2.917	151.2	S	02	12	21.15	0.20	-	-	-	-	I-2
APA0	9.623	252.7	P	02	13	17.14	1.50	72.7	25.0	9.03	4.0	I-C
APA0	9.623	252.7	S	02	15	02.84	2.00	53.5	25.0	19.24	4.0	I-C
BJO	11.041	299.3	P	02	13	35.98	3.00	-	-	-	-	I-2
BJO	11.041	299.3	S	02	15	30.60	5.00	-	-	-	-	I-2
FINES	16.227	244.1	P	02	14	46.33	1.75	33.2	15.0	10.90	1.5	I-C
FINES	16.227	244.1	S	02	17	37.83	3.00	-	-	-	-	I-C
HFS	20.856	257.2	P	02	15	42.82	0.50	28.0	15.0	9.42	2.0	I-C
JOF	16.606	239.6	P	02	14	09.86	1.00	-	-	-	-	I
JOF	16.606	239.6	S	02	16	33.42	2.00	-	-	-	-	I
KAF	15.617	245.2	P	02	14	36.00	2.00	-	-	-	-	I-C
KBS	12.704	321.0	P	02	13	57.47	1.00	-	-	-	-	I-2
KBS	12.704	321.0	S	02	16	08.06	2.00	-	-	-	-	I-2
KEF	15.957	247.3	P	02	14	42.72	0.75	-	-	-	-	I
KEV	10.209	270.3	P	02	13	25.19	0.50	-	-	-	-	I
KEV	10.209	2703	S	02	15	13.18	2.50	-	-	-	-	I
KJN	13.664	248.0	P	02	14	12.32	2.00	-	-	-	-	I
KJN	13.664	248.0	S	02	16	39.60	2.00	-	-	-	-	I
KTK1	11.738	270.5	S	02	15	50.37	2.50	-	-	-	-	C
MOR8	16.141	269.4	P	02	14	41.42	1.50	-	-	-	-	C
NAO01	21.132	261.5	P	02	15	45.44	0.60	-	-	-	-	I
NB201	20.847	261.4	P	02	15	43.07	0.60	-	-	-	-	I-C
NC303	20.687	261.6	P	02	15	41.27	0.50	-	-	-	-	I

Station	Δ [˚]	AZI [˚]	Phase	Hour	Minute	Second	σ Time [s]	BAZ [˚]	σ BAZ [˚]	P [s/˚]	σ P [s/˚]	Remarks
NC602	21.021	260.6	P	02	15	44.57	0.50	-	-	-	-	-
NORES	21.021	260.6	P	02	15	44.55	0.50	37.1	15.0	10.08	1.2	I-C
NRIS	10.521	91.5	P	02	13	30.19	1.00	-	-	-	-	I-2-C
NRIS	10.521	91.5	S	02	15	19.35	1.50	-	-	-	-	I-2-C
NUR	17.395	244.2	P	02	15	02.00	2.00	-	-	-	-	I-C
PKK	17.853	243.5	P	02	15	07.90	1.50	-	-	-	-	I
PVF	17.033	242.6	P	02	14	58.18	1.50	-	-	-	-	I
SDF	11.703	260.7	P	02	13	45.17	1.00	-	-	-	-	I
SDF	11.703	260.7	S	02	15	50.75	2.00	-	-	-	-	I
SPITS	11.731	318.0	P	02	13	44.85	0.50	103.0	15.0	11.98	2.5	I-2-C
SPITS	11.731	318.0	S	02	15	45.45	1.50	95.0	15.0	19.86	2.5	I-2-C
SUF	15.173	246.8	P	02	14	31.29	1.00	-	-	-	-	I
SUF	15.173	247.8	S	02	17	13.10	3.00	-	-	-	-	I
TRO	12.730	276.7	S	02	16	15.40	2.50	-	-	-	-	C
VAF	15.915	252.2	S	02	17	29.83	2.00	-	-	-	-	I
VAF	15.915	252.2	P	02	14	41.05	1.50	-	-	-	-	I

Table 6.5.3. The new hypocenter solutions for the 16 August 1997 Kara Sea event as plotted in Fig. 6.5.6. Listed are the source parameters and the number of data used by HYPOSAT as defining for onset times (OT), backazimuths (BAZ), ray parameters (RP), and travel-time differences (TTD). In the header line, the maximum possible number of these parameters is given in parenthesis. WMF is the weighted mean misfit for all available travel-time observations and RMS was calculated from all defining onset times. An 'F' together with the estimated depth indicates that the depth was fixed by the program. 'M' indicates the used method: NA-B - the shakeNA with smallest misfit, NA-M - the mean of all solutions in the consistency region, and H - the HYPOSAT solution.

Model	Lat [°]	Lon [°]	D [km]	σ D [km]	Time	OT (36)	BAZ (7)	RP (7)	WMF (36)	RMS [s]	EE [km^2]	M
AK135	72.382	57.356	30.4	29.1 -31.6	02:11:02.85	36	7	7	2.63	4.61	-	NA-B
AK135	72.391	57.371	29.4	29.1 -31.6	02:11:02.65	36	7	7	2.64	4.60	-	NA-M
AK135	72.366	57.367	34.4 F	13.2 - 51.7	02:11:03.26	36	5	1	2.64	4.58	252	H
IASP91	72.365	57.342	35.0	32.1 - 36.0	02:11:03.37	36	7	7	2.83	4.97	-	NA-B
IASP91	72.373	57.360	34.2	32.1 - 36.0	02:11:03.21	36	7	7	2.84	4.99	-	NA-M
IASP91	72.288	57.246	37.3 F	18.5 - 62.2	02:11:04.12	29	5	1	2.89	2.69	247	H
BAREY	72.383	57.740	30.3	27.8 - 31.0	02:11:03.76	36	7	7	1.21	1.80	-	NA-B
BAREY	72.389	57.753	29.7	27.8 - 31.0	02:11:03.66	36	7	7	1.21	1.79	-	NA-M
BAREY	72.394	57.802	39.8	10.1	02:11:04.88	30	4	1	1.35	1.27	1858	H
BAREZ	72.427	57.868	21.5	21.1 - 24.5	02:11:02.91	36	7	7	1.66	3.67	-	NA-B
BAREZ	72.427	57.874	22.2	21.1 - 24.5	02:11:03.01	36	7	7	1.68	3.66	-	NA-M
BAREZ	72.342	57.644	15.9	7.6	02:11:02.80	28	4	1	1.56	1.32	402	H
COMB	72.331	57.616	17.6	5.2	02:11:03.01	35	5	1	0.90	1.27	238	H

Table 6.5.4. Hypocenter solutions for the 16 August 1997 event in the Kara Sea as published by international data centres and the event locations performed for comparison with our results. Listed are source parameters including the fixed depth, the number of as defining used P- and S-onset times, backazimuths (BAZ), ray parameters (P), and travel-time differences (TTD). In parenthesis the maximum possible number of for this solution available data is given, respectively, such values are not available for NEIC and ISC. RMS is calculated from the defining onset times, WMF is the weighted misfit for all possible travel-time observations (in case of data centre solutions for all onsets, for which residuals were published), and Δ gives the epicentral distance between this solution and the *comb* solution of Table 6.5.3. EE lists the size of the error ellipse as plotted in Fig. 6.5.6. For further details see text.

Model	Lat [°]	Lon [°]	D [km]	Time	P	S	BAZ	P	TTD	RMS [s]	WMF	Δ [km]	EE [km^2]
REB	72.6484	57.3517	0	02:10:59.9	5(5)	-(4)	3(5)	3(5)	-(3)	0.20	1.77	36.5	179
PDE	72.835	57.225	10	02:10:59.77	7(7)	-(3)	-(?)	-(?)	-(3)	1.42	0.93	57.8	963
ISC	72.6171	56.9353	10	02:10:59.18	13(13)	-(9)	-(?)	-(?)	-(6)	1.30	1.08	39.3	358
J-B	72.6272	57.7404	18	02:10:57.27	10(10)	6(6)	7(7)	7(7)	4(4)	5.31	2.41	44.4	642
PREM	72.4919	57.5754	18	02:11:02.04	10(10)	6(6)	7(7)	6(7)	4(4)	4.34	1.88	18.0	502
IASP91	72.6331	57.7468	18	02:11:00.22	10(10)	6(6)	7(7)	7(7)	4(4)	5.79	2.74	30.7	649
AK135	72.6253	57.7464	18	02:11:00.30	10(10)	6(6)	7(7)	7(7)	4(4)	5.26	2.52	33.2	533
BAREY	72.5378	57.7625	18	02:11:02.55	10(10)	6(6)	7(7)	7(7)	4(4)	1.92	1.05	23.6	128
BAREZ	72.4819	57.7912	18	02:11:03.02	10(10)	6(6)	7(7)	7(7)	4(4)	3.80	1.53	17.9	262
COMB	72.4329	57.5582	18	02:11:03.35	10(10)	6(6)	7(7)	7(7)	4(4)	1.61	0.93	11.6	116

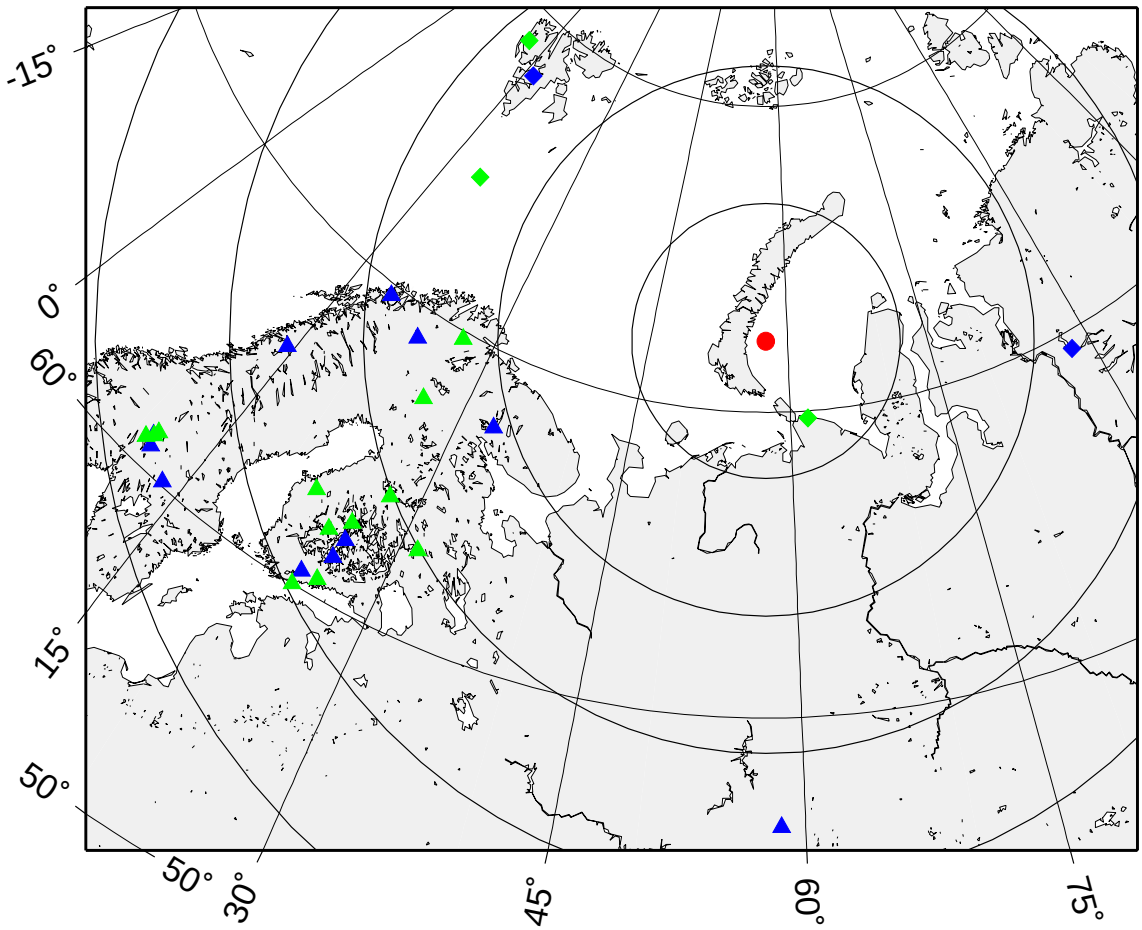

Figure 6.5.1: *Seismic stations (triangles and diamonds) which observed the Kara Sea event of 16 August 1997 (red point). Triangles (diamonds) were used for stations for which model barey (barez) gave the best results when calculating travel times for the joint model 'comb'. Blue symbols show stations, which contributed with parameter data to the bulletins of the international data centres, and green symbols represent stations with additionally analyzed data (this study). The circles show distances from the event in steps of 500 km.*

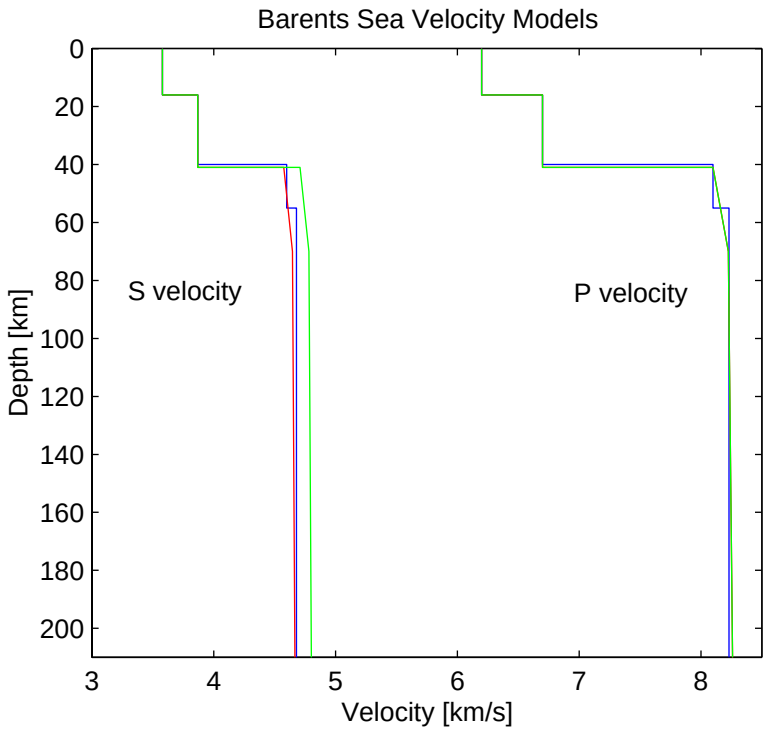

Figure 6.5.2: *Plot of regional velocity models used in this study. The models barey (red) and barez (green) were both derived from the barents model (blue, Kremenetskaya et al., 2001).*

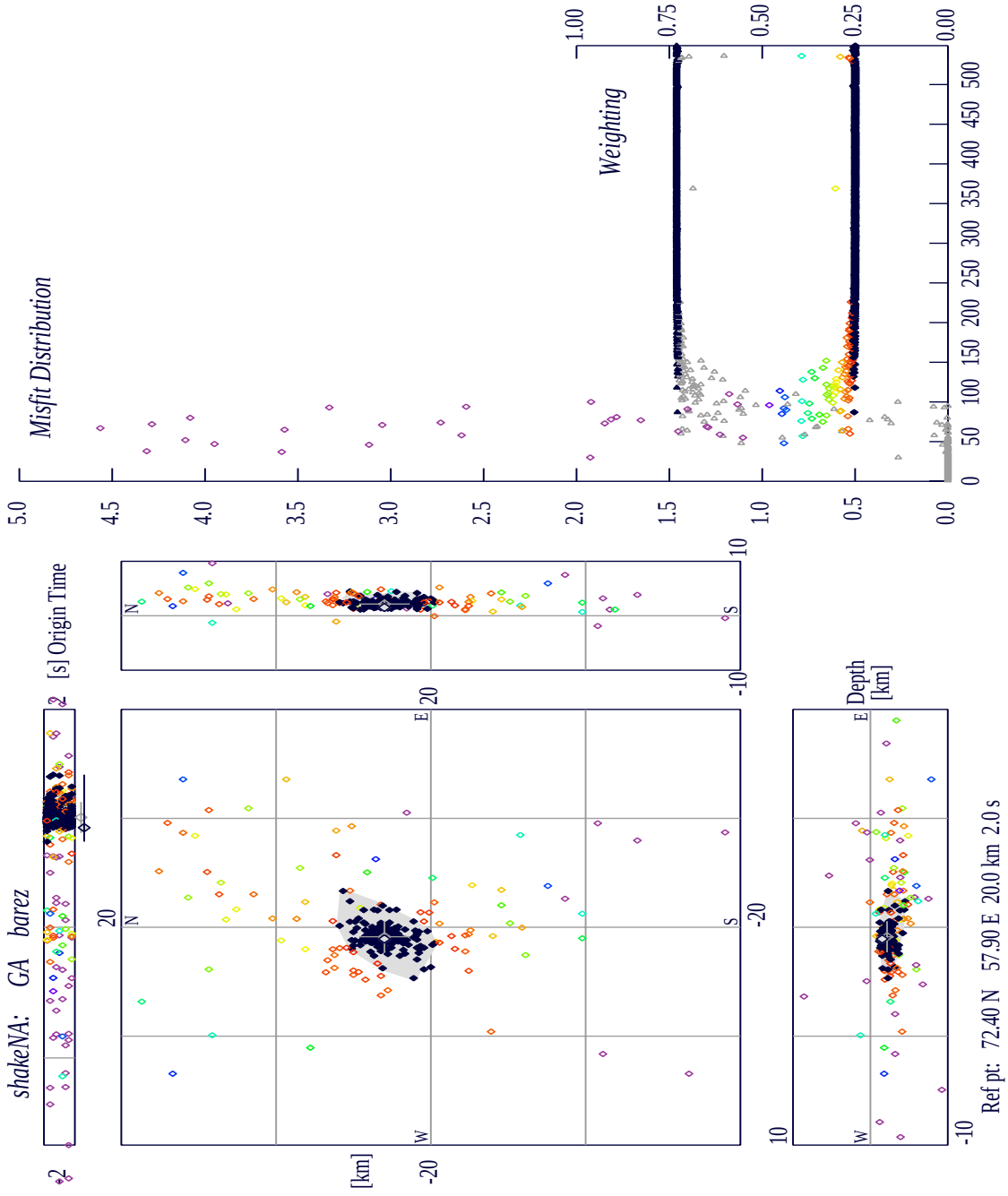

Figure 6.5.3: *Progress of the shakeNA program to a location estimate for the barez model shown as a map view and depth slices around the central portion of the sampled region.. The misfits are colour coded and the region of acceptable misfits is indicated with black symbols. The estimate of the consistency region associated with these acceptable models is indicated with grey shading. The right hand panel shows the misfit distribution and the approach to convergence. New models are generated as the iterations proceed and not all are as good as earlier models.*
The ensemble properties indicated by the grey marker and cross give a good indication of the location and its uncertainities.

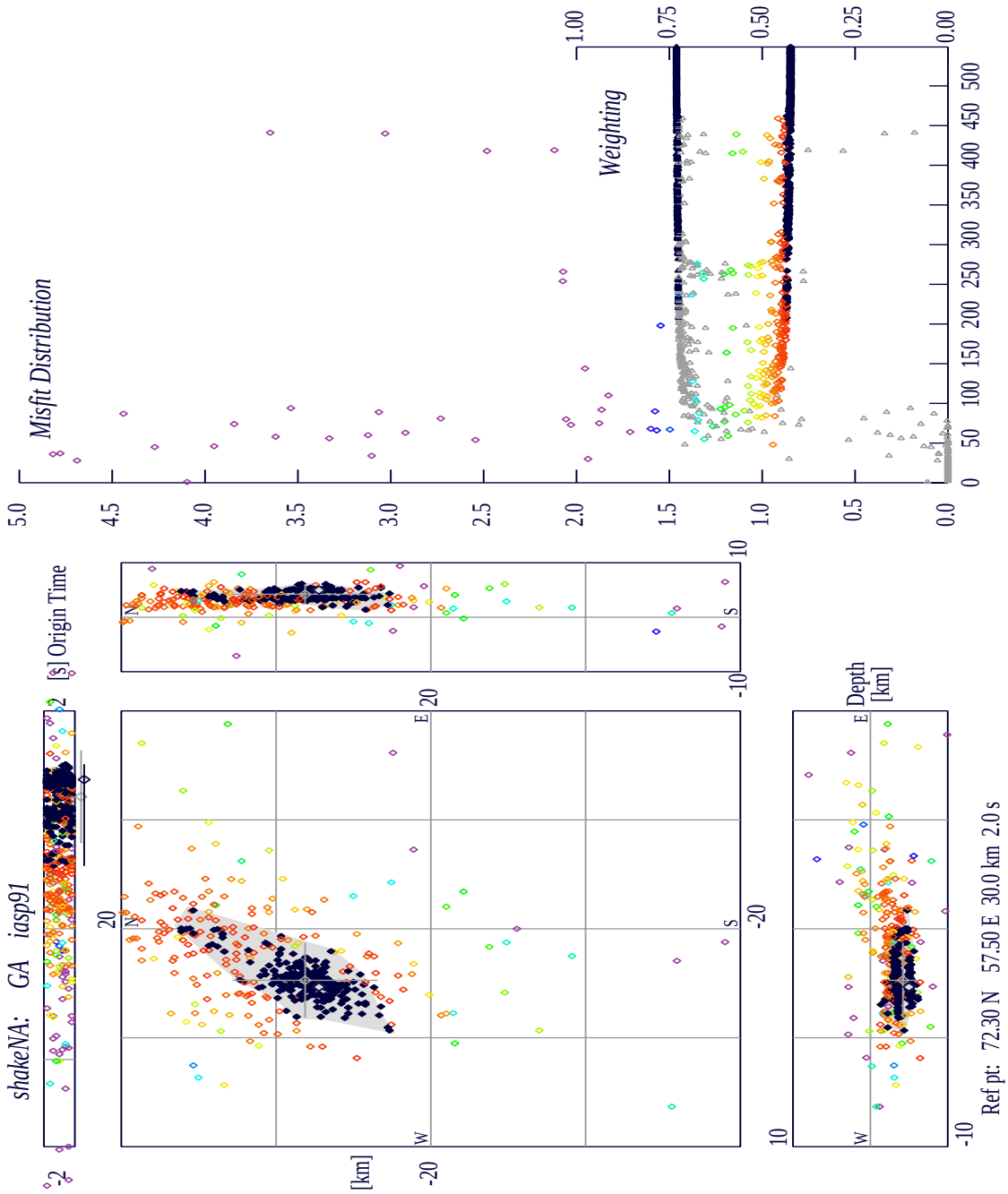

Figure 6.5.4: *same as Fig. 6.5.3 for model IASP91.*

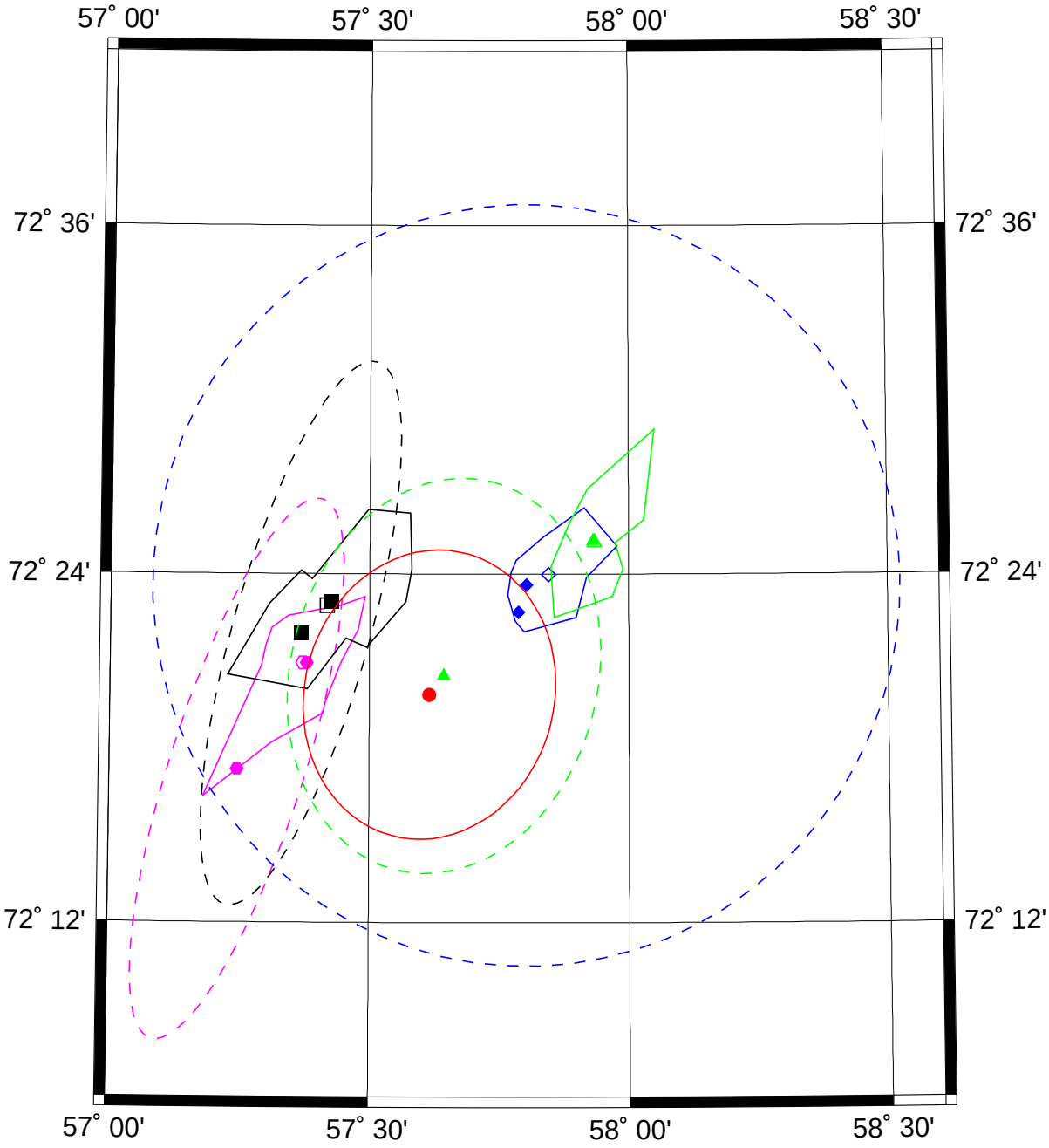

Figure 6.5.5: *Shows the NA (polygons) and the HYPOSAT (error ellipses) inversion results for the full data set and the different velocity models IASP91 (black), AK135 (magenta), barez (blue), barey (green), and 'comb' (red). For more details see text and Table 6.5.3.*

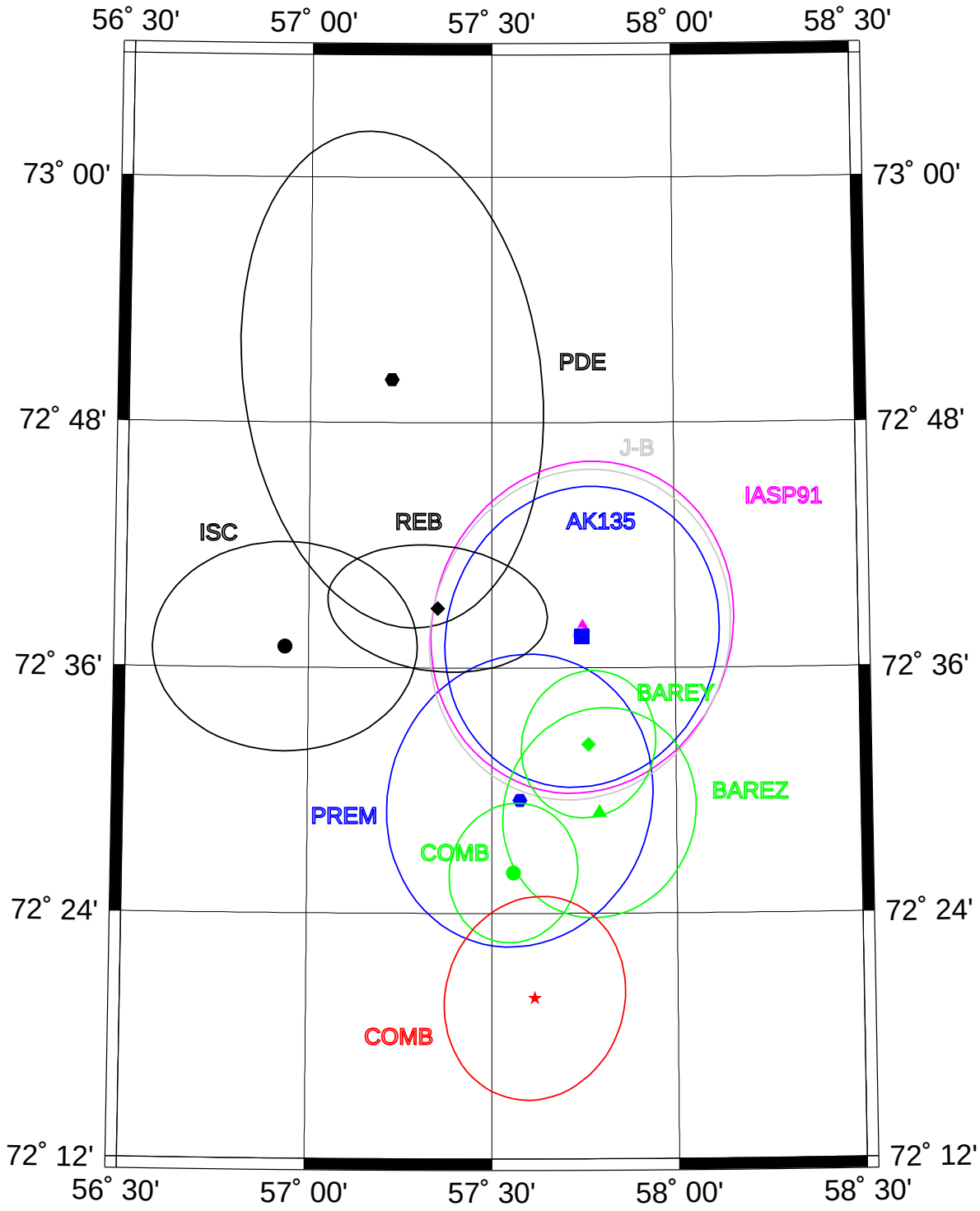

Figure 6.5.6: *Epicenters and error ellipses for the Kara Sea event of 16 August 1997 as published by data centres, and as estimated by our relocation experiment using only a limited set of data. For more details see text.*